International Journal of Aeronautical and Space Sciences (2020) 21:826–835
https://doi.org/10.1007/s42405-020-00299-y

IJASS International Journal of Aeronautical and Space Sciences

ORIGINAL PAPER

Computational Issues in Sparse and Dense Formulations of Integrated Guidance and Control with Constraints

Tae-Hun Kim[1] · Jongho Park[2] · Jong-Han Kim[3]

Received: 15 February 2020 / Revised: 1 June 2020 / Accepted: 9 June 2020 / Published online: 3 July 2020

Abstract
An integrated guidance and control problem under state constraints is considered for terminal homing of missile engagement. The problem is formulated as a moderate-size convex optimization problem, which can be efficiently solved via existing techniques such as interior point methods or alternating direction method of multipliers. Two different formulations are presented, and their computation time is investigated. We address computational issues that arise in implementing the optimization solvers on-board, and discuss several problem-specific hands-on techniques that help reducing the computational complexity and accelerating the convergence of the optimization algorithms.

Keywords Integrated guidance and control · Convex optimization · State constraints · Primal–dual interior point method

1 Introduction

In missile systems, a seeker subsystem plays a crucial role in terminal homing. It tracks a target continuously after acquisition and provides the measurements of the target motion [1]. If a strapdown seeker is considered, the target must be maintained inside the seeker's field of view. Therefore, look angle should be limited within feasible region. Also, if an agile turn maneuver against high-speed targets is considered, image distortion such as motion blur may occur in the image plane of a seeker. Then, it is highly probable that the seeker loses the target, resulting in the mission failure. Thus, look angle rate limitation must be considered to prevent the image distortion. Optimal guidance problems considering the look angle constraints have been proposed recently [2–7]. However, these studies deal with the lead angle constraints instead of directly restricting the look angle, hence assuming small angle of attack. This causes significant problems in the high maneuver cases where the angle of attack is not ignorable. Therefore, a need for advanced techniques that can directly handle the look angles arises.

Integrated guidance and control design becomes more and more popular to improve a missile system performance such as the accuracy of the interceptor and its kill envelope extension. Menon and Ohlmeyer [8] employed feedback linearization technique to integrated guidance and control. The proposed technique provided a stabilizing control law which was optimal with respect to an infinite-time performance index. Shima et al. [9] applied sliding mode control approach for the derivation of the integrated guidance–control algorithm. The sliding surface was defined using the zero-effort miss distance, obtained from a linearized differential game formulation. Idan et al. [10] also used sliding mode control methodology to control missile by two aerodynamics surfaces. It was shown that the integrated system could account simultaneously for the guidance and autopilot requirements using the additional degree of freedom. Smooth second-order sliding mode control was adopted by Shtessel and Tournes [11] against maneuvering target. The target acceleration was reconstructed in finite time, and smooth flight path angle, angle of attack, and pitch rate commands were generated. On the other hand, Xin et al. [12] presented an infinite-horizon

✉ Jong-Han Kim
jonghank@khu.ac.kr

Tae-Hun Kim
thkim1219@add.re.kr

Jongho Park
parkjo05@ajou.ac.kr

[1] Agency for Defense Development, 160, Bugyuseong-daero 488 beon-gil, Yuseong-gu, Taejon 34060, Republic of Korea

[2] Department of Military Digital Convergence, Ajou University, Yeongtong-gu, 206, World cup-ro, Suwon 16499, Republic of Korea

[3] Department of Electronic Engineering, Kyung Hee University, 1732, Deogyeong-daero, Giheung-gu, Yongin 17104, Republic of Korea

optimal control problem which was solved by θ-D technique. The method produced an approximate closed-form feedback controller in which online computation was not required. Vaddi et al. [13] developed a numerical approach using state-dependent Riccati equation methodology. State-dependent system matrices were obtained as the solution to a constrained least-squares optimization problem, and the target interception was modeled as a tenth-order nonlinear regulation problem. State-dependent Riccati equation approach was also used by Zhao et al. [14] for ground-fixed target with desired terminal impact angle. A time-varying state weighting matrix defined by functions of altitude-to-go was suggested to achieve a satisfactory terminal accuracy. Furthermore, Kim et al. [15] formulated an optimization problem with affine dynamic constraints. The optimal solution was derived as a time-varying state feedback control with a feedforward term, and the quadratic weighting functions were appropriately chosen.

In this study, an integrated guidance and control method considering state constraints for terminal homing is proposed. Short-period dynamics and guidance kinematics of a missile as well as actuator dynamics are considered [16,17]. The problem is formulated as a standard equality and inequality constrained quadratic problem that can be efficiently solved via existing techniques. The equality constraint consists of the discrete-time state space model of the missile dynamics. On the other hand, the inequality constraint consists of three limitations: acceleration, look angle, and look angle rate. Acceleration constraint must be considered because of the finite maneuver capability of the missile. Also, look angle constraint is considered due to the limitation of seekers image plane. Finally, look angle rate constraint is considered to prevent image distortion or signal intensity reduction of seeker system especially for high maneuver interception scenarios. Two different formulations are presented, and their computation time is compared for real implementation. Monte Carlo simulation is also carried out to verify the performance of the proposed algorithm.

The problem without the equality and inequality constraints has an elegant explicit solution which can be derived from the classical linear quadratic regulator theories or the dynamic programing approaches [15]. However, this is not the case for the problem we focus in this study, and the control solution should be obtained online via solving the finite horizon optimization problem at every time step. The primal–dual interior point method [18–21] is introduced with sparse matrix handling [22] and matrix caching, to efficiently solve the constrained quadratic problem on-board.

The paper is organized as follows: Sect. 2 formulates the integrated guidance and control problem considered in this study. In Sect. 3, primal–dual interior point method is presented, and numerical simulation results are shown in Sect. 4. Finally, the conclusion is given in Sect. 5.

2 Integrated Guidance and Control Formulation

2.1 Problem Description

A two-dimensional terminal homing problem in the vertical plane is considered as shown in Fig. 1. And, Fig. 2 shows positive definition of angles used in this study. $X_I - Z_I$ is a reference coordinate system whose origin is located at the missile's initial center of gravity. It is assumed that the missile is close to a collision triangle at the beginning of the terminal homing, and the missile and target deviations during the terminal homing are sufficiently small. Therefore, linearization can be performed around the initial Line-Of-Sight (LOS), λ_0, whose coordinate system is $X_{L0} - Z_{L0}$ as shown in Figs. 1 and 2. Also, constant known speed is assumed for both the missile and the target. x_b is a body-fixed coordinate system of the missile, and z_m is a relative displacement between the missile and the target normal to the initial LOS. R and λ are range-to-go and LOS of the missile and the target, respectively. Furthermore, v_m, α_m, and γ_m are speed, angle of attack, and flight path angle of the missile, respectively. a_m and a_t are accelerations of the missile and the target, respectively, normal to the LOS as shown in Fig. 1. ϵ_m and θ_m are look angle and pitch angle of the missile, respectively, whereas v_t is speed of the target. Finally, g is a gravitational acceleration which is parallel to Z_I.

The main objective of the terminal homing is to have the missile intercept the target, while limiting its maneuver acceleration by $|a_m| \leq a_{\max}$, the look angle by $|\epsilon_m| \leq \epsilon_{\max}$, and the look angle rate by $|\dot{\epsilon}_m| \leq \dot{\epsilon}_{\max}$. Also, we consider a rather challenging and restrictive but reasonable situation where the amount of time allowed for the terminal homing phase is insufficient because of the restrictions given by the mission operational requirements or the limits imposed by the other subsystems such as the seekers or the navigation related sensors, and so on. This implies that the conventional separate guidance and control techniques may not be able to achieve the satisfactory homing performance.

The short period dynamics of the missile is governed by the following equation.

$$\begin{bmatrix} \dot{\alpha}_m \\ \dot{q}_m \end{bmatrix} = \begin{bmatrix} Z_\alpha & 1 \\ M_\alpha & M_q \end{bmatrix} \begin{bmatrix} \alpha_m \\ q_m \end{bmatrix} + \begin{bmatrix} Z_\delta \\ M_\delta \end{bmatrix} \delta_m, \tag{1}$$

where q_m is a pitch rate, δ_m is a control fin deflection angle, and $Z_\alpha, Z_\delta, M_\alpha, M_q$, and M_δ are corresponding dimensional derivatives of the missile [16,17]. Now, a_m can be expressed as follows:

$$a_m = v_m(\dot{\alpha}_m - q_m) = v_m Z_\alpha \alpha_m + v_m Z_\delta \delta_m. \tag{2}$$

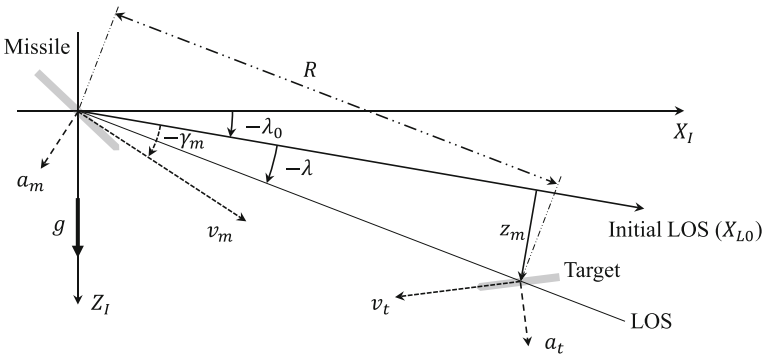

Fig. 1 Engagement geometry

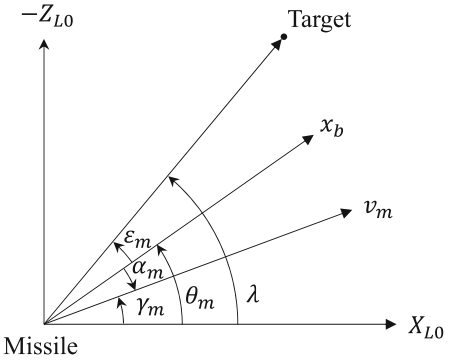

Fig. 2 Positive angle definition

And, the control fin actuator dynamics is modeled as a single lag system as follows:

$$\dot{\delta}_m = -\omega_a \delta_m + \omega_a \delta_c, \tag{3}$$

where δ_c is a control command, and ω_a is an inverse of the actuator time constant.

On the other hand, the kinematics describing the trajectory of the missile is given as follows:

$$\begin{bmatrix} \dot{\gamma}_m \\ \dot{z}_m \end{bmatrix} = \begin{bmatrix} 0 & 0 \\ v_m & 0 \end{bmatrix} \begin{bmatrix} \gamma_m \\ z_m \end{bmatrix} + \begin{bmatrix} -1/v_m \\ 0 \end{bmatrix} a_m, \tag{4}$$

where a_m can be replaced by (2). Using (1) and (3)–(4), an augmented system of equations is built as follows:

$$\underbrace{\begin{bmatrix} \dot{\delta}_m \\ \dot{\alpha}_m \\ \dot{q}_m \\ \dot{\gamma}_m \\ \dot{z}_m \end{bmatrix}}_{\equiv \dot{\bar{x}}} = \underbrace{\begin{bmatrix} -\omega_a & 0 & 0 & 0 & 0 \\ Z_\delta & Z_\alpha & 1 & 0 & 0 \\ M_\delta & M_\alpha & M_q & 0 & 0 \\ -Z_\delta & -Z_\alpha & 0 & 0 & 0 \\ 0 & 0 & 0 & v_m & 0 \end{bmatrix}}_{\equiv \bar{A}} \underbrace{\begin{bmatrix} \delta_m \\ \alpha_m \\ q_m \\ \gamma_m \\ z_m \end{bmatrix}}_{\equiv \bar{x}} + \underbrace{\begin{bmatrix} \omega_a \\ 0 \\ 0 \\ 0 \\ 0 \end{bmatrix}}_{\equiv \bar{B}} \underbrace{\delta_c}_{\equiv \bar{u}}. \tag{5}$$

The above equation can be discretized with the sampling interval of Δt.

$$x_{k+1} = Ax_k + Bu_k + b, \tag{6}$$

where the subscripts represent the time index, and the discretized matrices are obtained by $A = e^{\Delta t \tilde{A}}$, $B = \left(\int_0^{\Delta t} e^{\tau \tilde{A}} \mathrm{d}\tau\right) \tilde{B}$, and $b = \left(\int_0^{\Delta t} e^{\tau \tilde{A}} \mathrm{d}\tau\right) \tilde{b}$.

Now, we look at the inequality constraints. Acceleration constraint is considered due to the finite maneuver capability of the missile, and it can be expressed using (2) as follows:

$$-a_{\max} \le v_m Z_\alpha \alpha_m + v_m Z_\delta \delta_m \le a_{\max}, \tag{7}$$

where $a_{\max}$ is an acceleration limit. Also, look angle constraint is considered because of the limitation of seeker's image plane, and it can be expressed using $\lambda = -z_m/R$ and angle definition in Fig. 2 as follows:

$$-\epsilon_{\max} \le -z_m/R - \alpha_m - \gamma_m \le \epsilon_{\max}, \tag{8}$$

where $\epsilon_{\max}$ is a look angle limit. Finally, look angle rate constraint is considered to prevent image distortion or signal intensity reduction of the seeker, and it can be obtained by taking the derivative of the look angle with respect to time.

$$-\dot{\epsilon}_{\max} \le -v_m \gamma_m/R - z_m(v_m + v_t)/R^2 - q \le \dot{\epsilon}_{\max}, \tag{9}$$

where $\dot{\epsilon}_{\max}$ is a look angle rate limit, and $\dot{R}$ is approximated as follows:

$$\dot{R} \approx -(v_m + v_t). \tag{10}$$

Note that (7)–(9) consist of linear combinations of the state variables of (6). And the following set of linear time-varying constraints can be established.

$$\underbrace{\begin{bmatrix} v_m Z_\delta & v_m Z_\alpha & 0 & 0 & 0 \\ -v_m Z_\delta & -v_m Z_\alpha & 0 & 0 & 0 \\ 0 & -1 & 0 & -1 & 1/R_k \\ 0 & 1 & 0 & 1 & -1/R_k \\ 0 & 0 & -1 & -v_m/R_k & -(v_m+v_t)/R_k^2 \\ 0 & 0 & 1 & v_m/R_k & (v_m+v_t)/R_k^2 \end{bmatrix}}_{\equiv C_k} \times \begin{bmatrix} \delta_m \\ \alpha_m \\ q_m \\ \gamma_m \\ z_m \end{bmatrix} \leq \underbrace{\begin{bmatrix} a_{\max} \\ a_{\max} \\ \epsilon_{\max} \\ \epsilon_{\max} \\ \dot{\epsilon}_{\max} \\ \dot{\epsilon}_{\max} \end{bmatrix}}_{\equiv D}, \tag{11}$$

where R_k is the range-to-go after k samples. C_k in (11) is time-varying due to R_k. However, it can be easily predicted in the constant speed terminal homing phase where the curvature of the trajectory is sufficiently mild. Therefore, the range to go decreases almost linearly. For example, if the current range-to-go, R_0, is obtained from the inertial navigation system or from the seeker, then the range-to-go after k samples can be simply predicted by $R_0 - k(v_m + v_t)\Delta t$.

Therefore, the optimal control for $0 \leq t \leq t_f$ can be obtained via solving the following problem.

$$\begin{aligned} \underset{u_0,\ldots,u_{N-1}}{\text{minimize}} \quad & u_0^T R_0 u_0 + \sum_{k=1}^{N-1} \left(x_k^T Q_k x_k + u_k^T R_k u_k \right) \\ & + x_N^T Q_N x_N \\ \text{subject to} \quad & x_{k+1} = A x_k + B u_k \\ & C_k x_k \leq D, \end{aligned} \tag{12}$$

for all $k \in \{0, \ldots, N-1\}$, where the weighting matrices satisfy $Q_1, \ldots, Q_N \geq 0$ and $R_0, \ldots, R_{N-1} > 0$. The length of the horizon, N, is equal to $N = t_f/\Delta t$.

2.2 Sparse Formulation

Let us define y as follows:

$$y = [u_0^T \; x_1^T \; u_1^T \; x_2^T \; \ldots u_{N-1}^T \; x_N^T]^T. \tag{13}$$

Now, (12) can be transformed to a standard equality and inequality constrained quadratic problem as follows:

$$\begin{aligned} \underset{y}{\text{minimize}} \quad & y^T \mathcal{Q} y \\ \text{subject to} \quad & \mathcal{A} y = \mathcal{B} \\ & \mathcal{C} y \leq \mathcal{D}, \end{aligned} \tag{14}$$

where

$$\mathcal{Q} = \begin{bmatrix} R_0 & & & & \\ & Q_1 & & & \\ & & \ddots & & \\ & & & R_{N-1} & \\ & & & & Q_N \end{bmatrix}, \tag{15}$$

$$\mathcal{A} = \begin{bmatrix} B & -I & & & & \\ A & B & -I & & & \\ & & \ddots & & & \\ & & & A & B & -I \\ & & & & A & B & -I \end{bmatrix}, \tag{16}$$

$$\mathcal{C} = \begin{bmatrix} 0 & C_1 & & & \\ & 0 & C_2 & & \\ & & \ddots & & \\ & & & 0 & C_{N-1} \\ & & & & 0 & C_N \end{bmatrix}, \tag{17}$$

$$\mathcal{B} = \begin{bmatrix} -Ax_0 \\ 0 \\ \vdots \\ 0 \end{bmatrix}, \qquad \mathcal{D} = \begin{bmatrix} D \\ D \\ \vdots \\ D \end{bmatrix}. \tag{18}$$

2.3 Dense Formulation

Similar to the sparse formulation presented in the previous section, the dense formulation also starts from (12). Let us define X and U as follows:

$$X = [x_1^T \; x_2^T \; \ldots x_N^T]^T, \tag{19}$$

$$U = [u_0^T \; u_1^T \; \ldots u_{N-1}^T]^T. \tag{20}$$

Equality constraint in (12) can be listed as follows:

$$\begin{aligned} x_1 &= Ax_0 + Bu_0, \\ x_2 &= A^2 x_0 + ABu_0 + Bu_1, \\ &\vdots \\ x_N &= A^N x_0 + A^{N-1} B u_0 + A^{N-2} B u_1 + \cdots + B u_{N-1}. \end{aligned} \tag{21}$$

The above equations are rewritten in matrix form using X and U as follows:

$$X = X_0 + FU, \tag{22}$$

where

$$F = \begin{bmatrix} B & & & \\ AB & B & & \\ A^2B & AB & B & \\ \vdots & \vdots & & \ddots \\ A^{N-1}B & A^{N-2}B & \cdots\cdots & B \end{bmatrix}, \quad X_0 = \begin{bmatrix} Ax_0 \\ A^2x_0 \\ A^3x_0 \\ \vdots \\ A^Nx_0 \end{bmatrix}. \tag{23}$$

On the other hand, performance index in (12) can be expressed as follows:

$$J = U^T RU + X^T QX, \tag{24}$$

where

$$R = \begin{bmatrix} R_0 & & & \\ & R_1 & & \\ & & \ddots & \\ & & & R_{N-1} \end{bmatrix}, \quad Q = \begin{bmatrix} Q_1 & & & \\ & Q_2 & & \\ & & \ddots & \\ & & & Q_N \end{bmatrix}. \tag{25}$$

This performance index can be represented as a function of U using (22) as

$$J = U^T(F^T QF + R)U + 2X_0^T QFU + X_0^T QX_0. \tag{26}$$

Also, inequality constraint in (12) can be expressed using X as follows:

$$\bar{C}X \le \bar{D}, \tag{27}$$

where

$$\bar{C} = \begin{bmatrix} C_1 & & & \\ & C_2 & & \\ & & \ddots & \\ & & & C_N \end{bmatrix}, \qquad \bar{D} = \begin{bmatrix} D \\ D \\ \vdots \\ D \end{bmatrix}. \tag{28}$$

Similarly, the inequality constraint can be represented as a function of U using (22) as

$$\bar{C}FU \le \bar{D} - \bar{C}X_0. \tag{29}$$

Let us define the following variables:

$$J_1 = F^T QF + R, \tag{30}$$
$$J_2 = 2X_0^T QF, \tag{31}$$
$$I_1 = \bar{C}F, \tag{32}$$
$$I_2 = \bar{D} - \bar{C}X_0. \tag{33}$$

Finally, (12) can be transformed to a standard inequality constrained quadratic problem using (30)–(33) as follows:

$$\begin{aligned} \underset{U}{\text{minimize}} \quad & U^T J_1 U + J_2 U \\ \text{subject to} \quad & I_1 U \le I_2. \end{aligned} \tag{34}$$

Comparing the two different formulations, we note that there is a trade-off between the number of variables and sparsity. The sparse formulation deals with $6N$ variables, whereas the dense formulation deals with only N variables. While $\mathcal{Q}$ in (14) is block diagonal, J_1 in (34) is dense, which leads to sparsity reduction of matrix S_2 explained in the following section.

3 Primal–Dual Interior Point Method

In solving the problem in (14) of the sparse formulation, we apply the primal–dual interior point technique [18] whose search direction from a strictly feasible point (y, λ, ν) is given from the modified KKT condition by

$$\begin{bmatrix} 2\mathcal{Q} & \mathcal{C}^T & \mathcal{A}^T \\ -\text{diag}(\lambda)\mathcal{C} & -\text{diag}(f) & 0 \\ \mathcal{A} & 0 & 0 \end{bmatrix} \begin{bmatrix} \Delta y \\ \Delta\lambda \\ \Delta\nu \end{bmatrix} = - \begin{bmatrix} r_{\text{dual}} \\ r_{\text{cent}} \\ r_{\text{pri}} \end{bmatrix}, \tag{35}$$

where

$$\begin{bmatrix} r_{\text{dual}} \\ r_{\text{cent}} \\ r_{\text{pri}} \end{bmatrix} = \begin{bmatrix} 2\mathcal{Q}y + \mathcal{C}^T\lambda + \mathcal{A}^T\nu \\ -\text{diag}(\lambda)f - (1/\beta)\mathbf{1} \\ \mathcal{A}y - \mathcal{B} \end{bmatrix}, \tag{36}$$

with $f = \mathcal{C}y - \mathcal{D}$, and the barrier approximation parameter $\beta > 0$. The one vector, $\mathbf{1}$, represents the appropriately sized column vector whose elements are all one.

Rearranging (35) and (36) gives

$$\begin{aligned} &\begin{bmatrix} 2\mathcal{Q} & \mathcal{C}^T & \mathcal{A}^T \\ \mathcal{C} & \text{diag}(\lambda)^{-1}\text{diag}(f) & 0 \\ \mathcal{A} & 0 & 0 \end{bmatrix} \begin{bmatrix} \Delta y \\ \Delta\lambda \\ \Delta\nu \end{bmatrix} \\ &= - \begin{bmatrix} 2\mathcal{Q}y + \mathcal{C}^T\lambda + \mathcal{A}^T\nu \\ f + (1/\beta)\text{diag}(\lambda)^{-1}\mathbf{1} \\ \mathcal{A}y - \mathcal{B} \end{bmatrix}, \end{aligned} \tag{37}$$

which can be further simplified by block elimination via the Schur complement as

$$\begin{aligned} &\underbrace{\begin{bmatrix} 2\mathcal{Q} - \mathcal{C}^T\text{diag}(f)^{-1}\text{diag}(\lambda)\mathcal{C} & \mathcal{A}^T \\ \mathcal{A} & 0 \end{bmatrix}}_{\equiv S_1} \begin{bmatrix} \Delta y \\ \Delta\nu \end{bmatrix} \\ &= - \underbrace{\begin{bmatrix} 2\mathcal{Q}y + \mathcal{A}^T\nu - (1/\beta)\mathcal{C}^T\text{diag}(f)^{-1}\mathbf{1} \\ \mathcal{A}y - \mathcal{B} \end{bmatrix}}_{\equiv r_1}. \end{aligned} \tag{38}$$

Note that this is possible since $\text{diag}(\lambda)^{-1}\text{diag}(f)$ is always invertible as long as the problem is strictly feasible. The above equation can be efficiently solved via the LDL factorization of $S_1 = PLDL^T P^T$ as

$$\begin{bmatrix} \Delta y \\ \Delta v \end{bmatrix} = -PL^{-T}D^{-1}L^{-1}P^T r_1, \tag{39}$$

$$\Delta\lambda = -\text{diag}(f)^{-1}\text{diag}(\lambda)\mathcal{C}\Delta y - \lambda - (1/\beta)\text{diag}(f)^{-1}\mathbf{1}, \tag{40}$$

with the approximation parameter β increasing in every iteration by

$$\beta = -6N\mu/f^T\lambda, \tag{41}$$

with some algorithm parameter $\mu > 0$, and $6N$ representing the number of rows of $\mathcal{C}$.

With similar procedure, the modified KKT condition for the problem in (34) of the dense formulation can be summarized as follows:

$$\underbrace{\left[2J_1\bar{C}^T\text{diag}(\bar{f})^{-1}\text{diag}(\lambda)\bar{C}\right]}_{\equiv S_2}\left[\Delta y\right], = -\underbrace{\left[2J_1 y + J_2^T - (1/\beta)\bar{C}^T\text{diag}(\bar{f})^{-1}\mathbf{1}\right]}_{\equiv r_2}, \tag{42}$$

where $\bar{f} = I_1 y - I_2$.

Note that the LDL decomposition must be carried out at every iteration due to changes of the primal and the dual variables. However, the permutation ordering matrix P can be cached for the entire iterations because the sparsity pattern of S_1 and S_2 stays the same, which implies that additional computation time saving can be achieved. Also note that, the LDL decomposition can be carried out very efficiently by exploiting the sparsity pattern of the reduced KKT matrices, S_1 and S_2. For this purpose, off-the-shelf sparse matrix computation libraries such as `SuiteSparse` [22] can be used. Figures 3 and 4 show sparsity pattern of S_1 and S_2, respectively, with the horizon size $N = 300$. Matrix S_2 does not have any zero element as shown in Fig. 4.

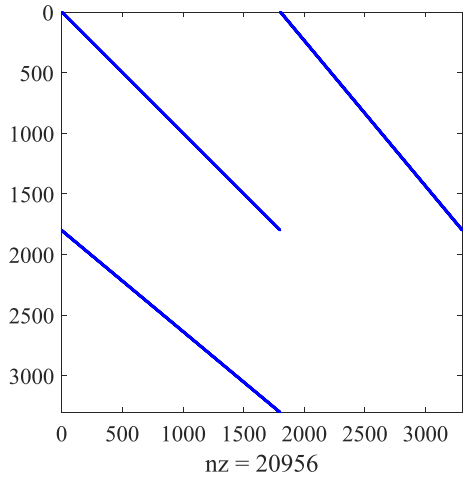

Fig. 3 Sparsity pattern of matrix S_1

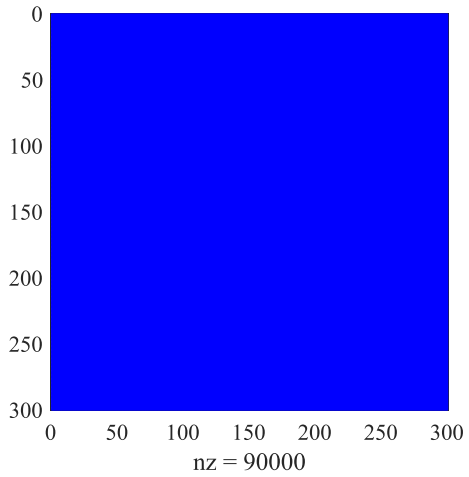

Fig. 4 Sparsity pattern of matrix S_2

Table 1 System parameters and design parameters

Z_α	$-2.9399/s$	v_m	510 m/s
Z_δ	$-0.6497/s$	$a_{\max}$	10 g
M_α	$-623.6149/s^2$	$\epsilon_{\max}$	4°
M_q	$-5/s$	$\dot{\epsilon}_{\max}$	$25°/s$
M_δ	$-554.4808/s^2$	ω_a	100/s
Q_k	diag([0 0 0 0 0])	for $k \in \{1, \ldots, N-1\}$	
Q_N	diag([0 0 0 0 1])		
R_k	1	for $k \in \{0, \ldots, N-1\}$	

4 Numerical Simulation

The performance of the proposed integrated guidance and control design is evaluated through numerical simulation. The total engagement time is 2.0 s and $\lambda_0 = 0°$. The parameters of the missile [9,16] is listed in Table 1. In Table 1, g is 9.8067 m/s^2 and the operator diag is a square diagonal matrix with the elements inside the square bracket on the main diagonal. The constant target speed, v_t, is set to 1000 m/s. The initial state variable of the missile is set to $[0°\ 0°\ 0°/s\ 2°\ 60m]^T$ where the order of the state is shown in (5).

To intercept the target, the fifth diagonal element in Q_N is assigned to nonzero number so that small z_m is to be achieved at the end of the terminal homing as shown in Table 1. The other diagonal elements in Q_k for $k \in \{1, \ldots, N\}$ are left zero because they are not required to be regulated.

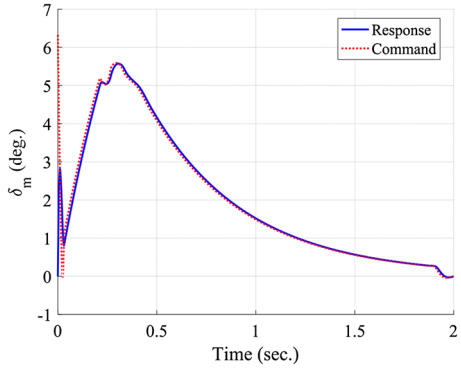

Fig. 5 Control input of the missile

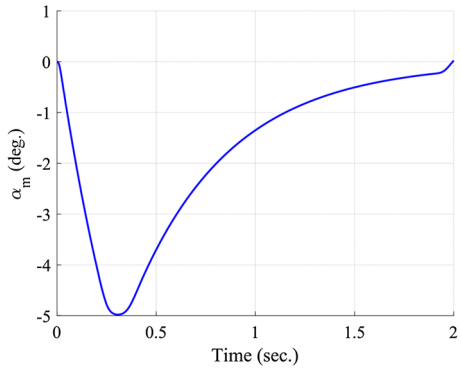

Fig. 6 Angle of attack of the missile

The same result is achieved using the sparse formulation and the dense formulation. Figures 5, 6, 7, 8 and 9 show the time responses of the state variables. In Fig. 5, solid line and dotted line represent δ_m and δ_c, respectively. The final miss distance of the proposed algorithm is $0.0005m$ as shown in Fig. 9. On the other hand, Figs. 10, 11 and 12 show the time responses of the acceleration, look angle, and look angle rate of the missile, respectively. And these variables stay within the considered limit (dotted line in Figs. 10, 11, 12) during the entire engagement, which means that the formulated problem gives the feasible solution satisfying the inequality constraints.

Note that, unlike the conventional separate guidance and control strategies, the proposed algorithm does not produce divergent acceleration command around the vicinity of the impact point which is the crucial part for the final miss distance as shown in Fig. 10. This implies that the proposed technique does not require any divergence-preventive techniques such as command freezing or nullifying [15]. Therefore, it can take full advantage of applying the optimal guidance and control until the last moment of the impact.

Computation time of two formulation methods presented in this study is evaluated and compared. For the platform, Intel Xeon E5-2670 CPU running at 2.60 GHz is used with 32.0 GB RAM in a 64-bit operating system. And, the algo-

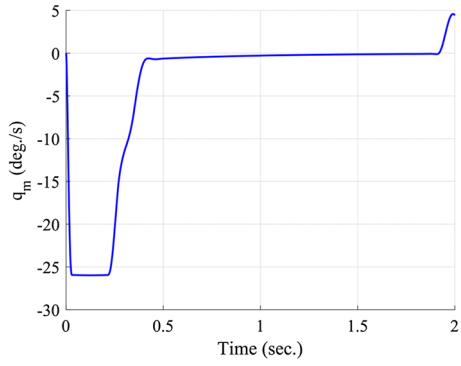

Fig. 7 Pitch rate of the missile

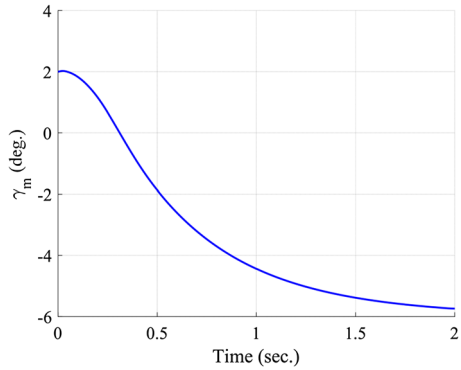

Fig. 8 Flight path angle of the missile

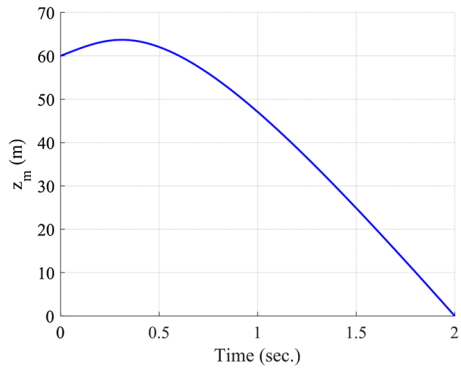

Fig. 9 Relative displacement between the missile and the target

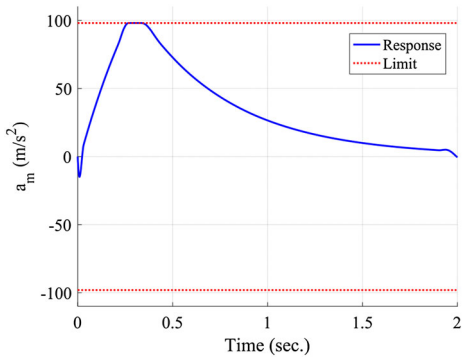

Fig. 10 Acceleration of the missile

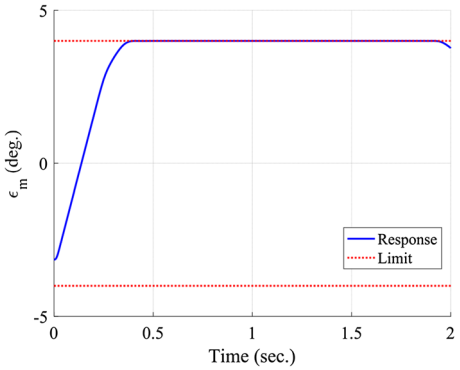

Fig. 11 Look angle of the missile

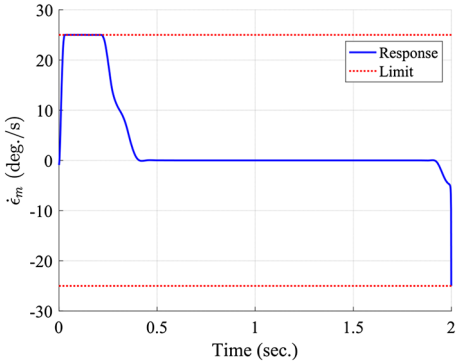

Fig. 12 Look angle rate of the missile

rithm is constructed on the Matlab R2016a software with quadprog solver from Matlab optimization toolbox [21].

For each case, simulation is conducted for 20 times and computation time is recorded only for solving the convex optimization problem (not the entire process). Table 2 shows the computation time of the sampling interval of 0.002 s, 0.01 s, and 0.05 s, respectively. As the sampling interval gets bigger, computation time reduces for both methods. When the sampling interval is very small, the computation time of the dense formulation is very long in particular, which makes it impractical for real-time implementation as shown in Table 2. However, when the sampling interval is relatively big, the dense formulation requires less calculation than the sparse formulation. This means that the horizon size of the considered problem has critical influence on the dense formulation in terms of computational burden.

Monte Carlo simulation is also employed to evaluate the performance of the proposed integrated guidance and control algorithm with different initial conditions of the missile. 500 sample runs are carried out with x_0 randomly chosen for each case. Note that the parameters including $a_{\max}$, $\epsilon_{\max}$, and $\dot{\epsilon}_{\max}$ in Table 1 are also applied in Monte Carlo runs. The simulation results are presented in Figs. 13, 14, 15, 16 and 17 from where it is shown that the proposed algorithm provides satisfactory performance. Acceptable final miss distances are

Table 2 Computation time evaluation

Formulation method	Δt	Average	Standard deviation
Sparse formulation	0.002	4.4089	0.3166
	0.01	0.4082	0.2965
	0.05	0.1243	0.2728
Dense formulation	0.002	90.0802	1.7857
	0.01	1.2267	0.2349
	0.05	0.1022	0.2374

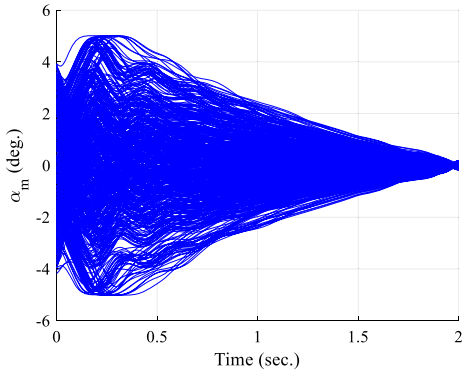

Fig. 13 Angle of attack of the missile (Monte Carlo simulation)

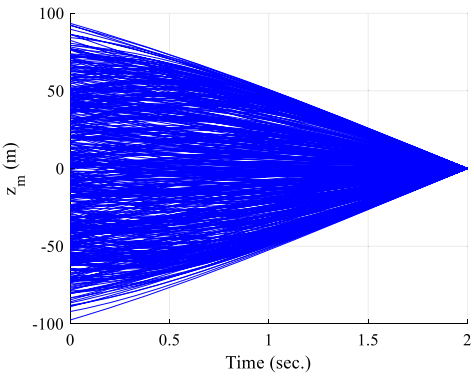

Fig. 14 Relative displacement between the missile and the target (Monte Carlo simulation)

achieved as shown in Fig. 14. Furthermore, the acceleration, look angle, and look angle rate of the missile are within the predefined limit for all cases, as shown in Figs. 15, 16 and 17.

5 Conclusions

An integrated guidance and control problem which considers the constraints on the maneuver acceleration, the look angle, and the look angle rate is presented in this study. The problem is of significant importance in practice because such constraints can guarantee the flight safety and the seeker performance under high maneuver situations. The problem is

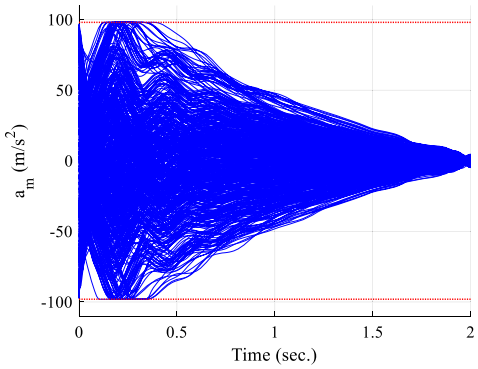

Fig. 15 Acceleration of the missile (Monte Carlo simulation)

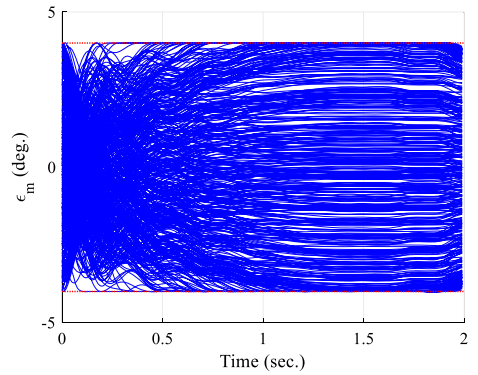

Fig. 16 Look angle of the missile (Monte Carlo simulation)

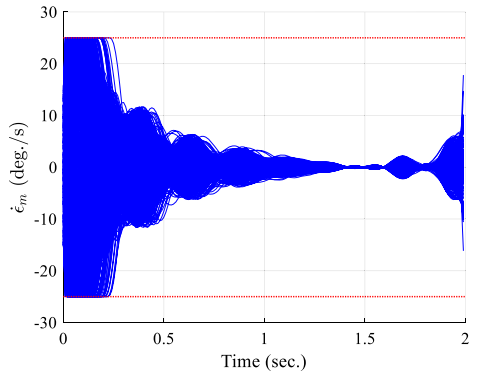

Fig. 17 Look angle rate of the missile (Monte Carlo simulation)

formulated as a standard quadratic problem in two ways, and the optimal control is obtained by solving the series of such problems at every time step. Moderate-sized problems can be efficiently solved via generic convex optimization solvers such as the family of interior point methods. The size of the problem we consider in this study grows with the horizon size, and the problem must to be solved on-board. To reduce the complexity in solving the primal–dual search direction, several numerical techniques, including the Schur complement, sparsity pattern exploitation, and permutation order caching, are mentioned.

For future research, the proposed integrated guidance and control algorithm will be extended to deal with three-dimensional space. Also, recent first-order methods such as the alternating direction method of multipliers will be applied.

Acknowledgements This work was partially supported by the National Research Foundation of Korea (NRF) grant funded by the Korea government (MSIT) (No.2019R1C1C1011579) and by a grant from Kyung Hee University in 2019 (KHU-20192291).

Compliance with Ethical Standards

Conflict of interest The authors declare that they have no conflict of interest.

References

1. Siouris G (2004) Missile guidance and control systems. Springer, New York, pp 102–112
2. Park BG, Kim TH, Tahk MJ (2013) Optimal impact angle control guidance law considering the seeker's field-of-view limits. Proc Inst Mech Eng Part G J Aerosp Eng 227(8):1347
3. Park BG, Kim TH, Tahk MJ (2016) Range-to-go weighted optimal guidance with impact angle constraint and seeker's look angle limits. IEEE Trans Aerosp Electron Syst 52(3):1241
4. Kim TH, Park BG, Tahk MJ (2013) Bias-shaping method for biased proportional navigation with terminal-angle constraint. J Guid Control Dyn 36(6):1810
5. Tekin R, Erer K (2015) Switched-gain guidance for impact angle control under physical constraints. J Guid Control Dyn 38(2):205
6. Ratnoo A (2016) Analysis of two-stage proportional navigation with heading constraints. J Guid Control Dyn 39(1):156
7. Park BG, Kwon HH, Kim YH, Kim TH (2016) Composite guidance scheme for impact angle control against a non-maneuvering moving target. J Guid Control Dyn 39(5):1132
8. Menon P, Ohlmeyer E (2001) Integrated design of agile missile guidance and autopilot systems. Control Eng Pract 9(10):1095
9. Shima T, Idan M, Golan OM (2006) Sliding-mode control for integrated missile autopilot guidance. J Guid Control Dyn 29(2):250
10. Idan M, Shima T, Golan O (2007) Integrated sliding mode autopilot-guidance for dual-control missiles. J Guid Control Dyn 30(4):1081
11. Shtessel YB, Tournes CH (2009) Integrated higher-order sliding mode guidance and autopilot for dual-control missiles. J Guid Control Dyn 32(1):79
12. Xin M, Balakrishnan SN, Ohlmeyer EJ (2006) Integrated guidance and control of missiles with θ-D method. IEEE Trans Control Syst Technol 14(6):981
13. Vaddi SS, Menon PK, Ohlmeyer EJ (2009) Numerical state-dependent riccati equation approach for missile integrated guidance control. J Guid Control Dyn 32(2):699
14. Zhao Y, Chen J, Sheng Y (2014) Terminal impact angle constrained guidance laws using state-dependent Riccati equation approach. Proc Inst Mech Eng Part G J Aerosp Eng 229(9):1616
15. Kim JH, Whang I, Kim B (2016) Finite horizon integrated guidance and control for terminal homing in vertical plane. J Guid Control Dyn 39(5):1104
16. Zarchan P (2012) Tactical and strategic missile guidance, 6th edn. American Institute of Aeronautics and Astronautics Inc, Reston, pp 473–527

17. Nelson RC (1998) Flight stability and automatic control, 2nd edn. WCB/McGraw-Hill, New York, pp 152–161
18. Boyd S, Vandenberghe L (2004) Convex optimization. Cambridge University Press, Cambridge, pp 324–615
19. Grant M, Boyd S(2014) CVX: Matlab software for disciplined convex programming, version 2.1. http://cvxr.com/cvx
20. Grant M, Boyd S (2008) Recent advances in learning and control. In: Blondel V, Boyd S, Kimura H (eds) Lecture notes in control and information sciences. Springer, Berlin, pp 95–110
21. The MathWorks (2016) Matlab optimization toolbox. The MathWorks, Natick
22. Davis TA, Hu Y (2011) The university of florida sparse matrix collection. ACM Trans Math Softw 38(1):1